Deep Learning Approaches to Autocorrelation Function and Signal-to-Noise Ratio Estimation in Noisy Images

Kai Liang Lew[1*], Kok Swee Sim[2], Shing Chiang Tan[3]

[1,2]Faculty of Engineering and Technology, Multimedia University, Jalan Ayer Keroh Lama, 75450 Bukit Beruang, Melaka, Malaysia

[3]Faculty of Information Science & Technology, Multimedia University, Jalan Ayer Keroh Lama, 75450 Bukit Beruang, Melaka, Malaysia

*corresponding author: (sksbg2022@gmail.com; ORCiD: 0000-0003-2976-8825)

Abstract – Accurate estimation of signal-to-noise ratio (SNR) in Scanning Electron Microscopy (SEM) is crucial because it evaluates the image quality. SEM images faced a challenge whereby Gaussian noise commonly appears in the images. Thus, researchers have developed several methods to estimate the SNR value. With the introduction of deep learning, most of the limitations in the classical methods can be addressed. This paper proposes a novel deep learning, CNN-based Calibration Map Network (CalibNet) to estimate the SNR value from SEM images using a calibration map between classical SNR and autocorrelation function SNR. The architecture consists of convolutional layers, rectified linear unit (ReLU) activations, max-pooling layers, adaptive pooling, and a regression head to predict the SNR value correctly. The proposed model is trained, validated and tested on two SEM images, the Biofilm SEM dataset (67 images) and the NFFA-EUROPE SEM dataset (961 images). Each image was artificially corrupted with Gaussian noise variance ranging from 0.001 to 0.01 to simulate realistic SEM imaging conditions. The proposed model was compared with Classical SNR, Autocorrelation Function (ACF), Nearest Neighbour (NN)-ACF, First-Order Linear Interpolation (LI)-ACF, and Quadratic-Sigmoid (Quarsig)-ACF methods. The results show that CalibNet outperformed all the classical methods in terms of mean absolute error (MAE), root mean square error (RMSE), mean absolute percentage error (MAPE) and R-squared (R^2). Statistical analyses further confirmed that CalibNet predictions closely align with the Classical SNR values. Future work includes exploring more advanced model architectures, alternative calibration techniques, and real-time SNR estimation applications.

Keywords— Scanning Electron Microscopy, Signal-to-Noise Ratio, Convolutional Neural Networks, Image Quality, Deep Learning, Calibration.

1. INTRODUCTION

Scanning Electron Microscope (SEM) produces high-resolution images by scanning a surface with focused electrons [1]. SEM imaging has shown its value in many sectors, including material science, biological research, and industrial semiconductor chip manufacturing. SEM images can capture the nanoscale details invisible to the naked eye, proving their value [2]. Chip production requires SEM imaging because it can help detect defective chips and examine microscopic components [3]. In biological research, SEM offers precise visualisation of cellular structures [4]. It can also help examine the material surface in a high-resolution visualisation.

The challenge that SEM imaging constantly faces is Gaussian noise in the images [5]. The Gaussian noise is white noise produced by the microscope's internal parts during image capture [6]. A poor-quality SEM image has a higher noise level because the noise corrupts the details [7]. The noises are everywhere in the images, and they overlap with the signal of the image, so the image quality is getting lower and lower [8]. Moreover, it will also cause the image to take longer to analyse, making it harder to interpret [9]. As the details of the image start to get smaller, there is nothing meaningful in the image [10]. The SNR is introduced to estimate the image's signal level to overcome the gap [11]. The SNR uses the ratio of the signal and noise to estimate the quality of the images [12]. The SNR produces a lower value if the noise value is higher than the signal noise. It will be vice versa if the noise value is lower than the signal noise. A good image quality has a high SNR value and a low noise level, which shows that SNR is good at checking the image quality. Therefore, many researchers have started using SNR to identify the image's noise level and improve their quality. The SNR has improved many filters, and the image can be denoise without losing the details.

Many researchers conducted studies regarding the noise problems in SEM images. Their interest has led them to create various filtering methods that help reduce noise. They have developed mathematical equations and foundational theories to support their work. The filters, such as Gaussian smoothing, median filtering, and adaptive filtering, can reduce the noise without damaging the details of the images. They are good at reducing noise, but they require an SNR value to perform optimally. The filters can sometimes over-smooth the images without a known SNR value because the details in the image are assumed to be the noise and removed. The filters without known SNR can greatly cause the image to lose value and make it hard to interpret. This impact causes the researcher to develop even more enhanced techniques to estimate the SNR to get a better, clearer SEM image and better noise reduction.

Classical approaches for estimating SNR values include patch-based estimation, Fourier-based analysis, wavelet-based methods, and autocorrelation-based approaches [13]. These are statistical methods because they rely on mathematical equations and manual calculations. When used on a large dataset, this usually leads to a longer computation time. Patch-based estimation techniques are suitable for analysing details in small image regions [14]. Fourier-based analysis methods perform differently from patch-based estimation because they convert the image into the frequency domain to estimate noise levels [15]. Wavelet-based methods require multiple scales of the image to analyse the noise and split it from important details [16]. Moreover, the autocorrelation-based approach converts the image into a centre-sliced one-dimensional (1d) autocorrelation to identify the peak value of the centre. It subtracts this from the original image's peak value to obtain the SNR value. All these methods show their strength in SNR and noise level estimation, but they often come with weaknesses. They need to manually configure their parameters and select the appropriate image regions, which can lead to human error and reduce the reliability in estimating SNR. Deep learning is introduced to address these manual configurations and the manual selection of image regions to improve the accuracy and reliability of SNR estimation.

Recent advancements in deep learning have developed many applications for image processing, including noise estimation and reduction. These applications show promising results in estimating the SNR values in SEM images [17]. Deep learning techniques significantly differ from the classical methods because they only need a model, a convolutional neural network (CNN) and a labelled dataset to perform the SNR estimation. They not only remove the usage of mathematical equations, but they can also self-learn based on the provided datasets and labels. The CNN is unique because of its ability to extract the image features automatically. Moreover, the existing deep learning methods usually focus on the denoising of images, which does not require knowing the SNR values [18]. In this paper, a novel deep learning model, Calibration Map Network (CalibNet), is explicitly designed to address this issue by estimating SNR accurately in SEM images. CalibNet uses a calibration map derived from classical and autocorrelation-based SNR methods to estimate SNR across a wide range of noise levels effectively. This method is unique because of the combination of the calibration map with the deep learning method. This shows that it is possible to do and the first to develop it.

In light of this, the first objective of this paper is to develop CalibNet that can accurately estimate SNR values in SEM images. The CalibNet is used for regression tasks because it only outputs a single estimation on a single image. These images are corrupted with Gaussian noise at variance levels ranging from 0.001 to 0.01. Each image is also resized into 256 x 256 pixels, so every image is standardised. The model is trained with a calibration map created using linear regression. This is because linear regression can give a suitable parameter for CalibNet to train. The parameter selection is based on the coefficient in classical and autocorrelation-based SNR calculations. This objective can address the limitations of classical methods and provide a reliable SNR estimation in SEM images.

The second objective is to prove that the proposal model can outperform the other classical methods. The proof is to evaluate the performance of the CalibNet by comparing it with other classical autocorrelation-based SNR estimation methods. The baseline for this paper is the classical SNR, which only uses a single image to estimate its SNR. The autocorrelation-based methods are the benchmark for the CalibNet because the training input of the CalibNet consists of ACF SNR, which is used in the calibration map. This makes the benchmarking relevant in comparison with the CalibNet.

The main research question is addressed based on below objective and contribution.

How accurate is the deep learning method that uses a calibration map as input for training to estimate the SNR value in SEM images?

1.1 Paper Contributions

One of the contributions of this paper is developing a deep learning model to estimate the SNR value closest to the classical SNR. This method can reduce the processing time and be reliable when estimating the SNR value compared to the classical methods.

The second contribution that can be found in this paper is a comprehensive evaluation of CalibNet's performance. It is compared with autocorrelation-based methods. A quantitative and statistical test has been performed to highlight the performance of the CalibNet. Two datasets are used to evaluate their performance. This shows the robustness of the CalibNet for automated and precise SNR estimation.

1.2 Paper Structure

The remainder of this paper is organised as follows. The Literature Review section reviews related work based on noise level and SNR estimation in SEM images. The Methodology section explains the proposed methodology for SNR estimation using CalibNet, providing a detailed explanation of the architecture and training procedures used to develop the model. The section on Experimental Results, Analysis, and Discussion highlights significant experimental outcomes, emphasising the advantages and limitations of the proposed paradigm. The section also examines the impact of these discoveries relative to other autocorrelation-based techniques, such as NN, LI, and QSE. The Conclusion summarises the whole paper and provides several suggestions for future work to expand this paper.

2.   LITERATURE REVIEW

This section compares classical and deep learning techniques for calculating SNR and noise levels by reviewing related work. While deep learning techniques use CNNs or other advanced models to carry out these estimates automatically, classical approaches usually depend on mathematical equations to calculate noise and SNR values.

2.1 Classical Methods

Classical techniques use mathematical equations to calculate images' SNR and noise levels. A patch-based noise level estimating technique capable of performing denoising the image blindly was presented by Liu et al. Their approach calculates noise levels from a single noisy image and then applies denoising. Experimental results indicated superior performance in accuracy and stability compared to other methods. [19] created a locally adaptive patch-based (LAPB)

denoising method in the wavelet domain that efficiently lowers noise while maintaining picture features; their findings indicate competitive performance compared to existing methods. [20] presented a new three-step fusion technique consisting of pre-estimation, fusion, and final computation. Their solution outperformed techniques like BM3D, DDID, MLP, and EPLL in peak signal-to-noise ratio (PSNR), structural similarity (SSIM), and visual quality by merging spatial and fractional Fourier domain findings from many denoising algorithms. [21] introduced three novel methods to estimate noise standard deviation directly from wavelet components and compared them with mean absolute deviation (MAD) methods. Their results indicated that these new methods provided more accurate noise-level estimations than the MAD approach. Lew et al. introduced a novel single-image SNR estimation technique, Quarsig SNR Estimation (QSE), which was designed explicitly for SEM images. This technique utilises the ACF to calculate peak values for both original and noisy images. Experimental findings demonstrated that QSE approximated actual SNR values, surpassing methods such as NN, LI, and their combination. [22] developed an SNR estimation method for SEM images using the piecewise cubic Hermite interpolation (PCHI) model. As demonstrated by asses including Cramer-Rao lower bound (CRLB), t-test, scatter plots, and Bland-Altman plots, their experimental comparisons showed better performance over other methods, including adaptive slope nearest neighbourhood (ASNN), linear least square regression (LLSR), and nonlinear least square regression (NLLSR). Table 1 shows the summary of the classical SNR methods from previous work.

Table 1. Summary of Classical SNR Methods from Previous Works

Authors	Method Name	Approach	Application	Performance / Results
[23]	Patch-based Noise Estimation Algorithm	Patch-based estimation	Blind denoising (single noisy image)	Superior accuracy and stability; outperformed other methods
[19]	Locally Adaptive Patch-based (LAPB)	Patch-based wavelet domain denoising	Image denoising	Effectively reduced noise, preserved image details; competitive results
[20]	Three-step Fusion Method	Fusion of spatial and fractional Fourier domains	Image denoising	High performance (PSNR, SSIM, visual quality); outperformed BM3D, DDID, MLP, EPLL
[21]	Wavelet-based noise estimation methods (vs. MAD)	Wavelet-based noise estimation	Estimating noise standard deviation	More accurate and robust than MAD; better noise estimation accuracy
[24]	QSE	ACF	SNR estimation in SEM images	Closest to actual SNR; outperformed NN, LI, and NN+LI methods
[22]	Piecewise Cubic Hermite Interpolation (PCHI)	Interpolation-based SNR estimation	SNR estimation in SEM images	Superior results (CRLB, t-test, scatter plot, Bland-Altman); outperformed ASNN, LLSR, NLLSR

2.2. Deep Learning Methods

Deep learning methods use CNN or other advanced models to estimate the noise level automatically and SNR in images. [25] proposed a two-step approach that uses a classifier, CNN, to detect the noise type and then denoise based on the detected noise type using a denoising autoencoder (DAE). Their classifier classified various types of noise with an accuracy of 98.2–100%, and the DAE model improved the PSNR and SSIM compared to other state-of-the-art models. [24] integrated convolutional feature extraction with a combination of deep wavelet machine learning classifiers in the related approach. Their model with support vector machine (SVM) archived 91.30% in accuracy and outperformed other machine learning classifiers. [26] adopted an alternative strategy by converting the images into histograms as training datasets. The dataset then feeds into the Gaussian-Noise Convolutional Neural Network (GN-

CNN) to classify the noise levels. This approach successfully differentiated the noise variance ranging from 0.001, 0.002 and 0.003 in the images with the F1 score of 93.97% and testing accuracy of 93.8%, outperforming other deep learning modes. [27] addressed single and mixed noise in images using dual-model architecture to classify the noise types and denoising based on the classification result. The architecture surpassed the existing methods by archiving high PSNR and SSIM values. [28] further expand the research with their Proposed System Architecture (PSA) to detect and identify the noise type in the given images. It can identify five types of noise: Gaussian noise, impulse noise, Poisson noise, and speckle noise. It had 99.25% accuracy in classifying the noise types and outperforming other models. [29] presented customised CNN architecture to classify three types of noise: Salt and pepper, Gaussian and Sinusoidal noise. Their proposed model achieved the highest accuracy in classifying the noise type and outperformed other classical methods. Table 2 shows the summary of deep learning based on recent studies.

Table 2. Summary of Deep Learning-based from Recent Studies

Authors	Method	Approach	Noise Types / Levels	Key Results
[11]	CNN Classifier + DAE	Two-step (Noise detection + Denoising)	Multiple noise types	98.2–100% classification accuracy; highest PSNR and SSIM compared to state-of-the-art methods
[12]	CNN + Wavelet + ML Classifier (SVM)	Two-step (Noise detection + Classification)	Multiple noise types	91.30% accuracy (SVM), outperforming other classifiers
[13]	GN-CNN	Noise variance classification using histogram-based CNN	Gaussian noise variance (0.001, 0.002, 0.003)	F1 Score: 93.97%; Accuracy: 93.8% (outperformed other models)
[14]	Two Deep Learning Models	Two-step (Classification + Denoising)	Single and mixed noise types	Higher classification accuracy; superior PSNR and SSIM values
[15]	Proposed System Architecture (PSA)	Deep learning-based noise detection and classification	Gaussian, Impulse, Poisson, Speckle	99.25% classification accuracy; superior performance
[16]	Customised CNN	CNN-based noise classification	Salt & Pepper, Gaussian, Sinusoidal	Highest classification accuracy; outperformed classical methods

2.3 Research Gap

Both classical and deep learning methods have shown their strength in estimating noise levels and SNR in images, but these methods still have limitations. The classical methods use mathematical equations to compute the estimation and require manual parameter tuning. Manually tuning parameters in classical methods is tedious and susceptible to human error. While existing deep learning methods can estimate noise levels, classify noise types, and perform image denoising automatically, they lack domain-specific calibration to estimate SNR.

This limitation restricts their accuracy and heavily depends on the provided datasets, which could lead to little exploration in estimation SNR. The development of deep learning-based SNR estimation using calibration maps can enhance SNR estimation in SEM imaging, making it more reliable for users and opening new avenues for exploration.

3.   RESEARCH METHODOLOGY

This section explains the details of the architecture used in CalibNet, allowing for a better understanding of reproducing the CalibNet. This section also describes the method used to generate a calibration map. The calibration map uses linear regression on the classical SNR and the ACF-based SNR to create the suitable parameter. Figure 1 shows the flowchart of the process in this paper.

3.1 CNN-based Calibration Map Network (CalibNet)

The CalibNet was developed to estimate the SNR value in SEM images. It uses the calibration map as the training input. The architecture of the CalibNet consists of three convolutional layers with ReLU activation functions, two max-pooling layers, an adaptive pooling layer, and a regression head. CalibNet uses grayscale, 256x256 pixel images as its inputs. The first convolutional layer has one input channel and 16 output channels with a kernel size of 3 and padding, followed by a ReLU and a max-pooling layer with a size of 2. The single input channel is to receive the input as a grayscale image. The ReLU is used to introduce non-linearity to the model. Max-pooling is used to reduce the spatial dimension. The second

convolution layer has the same configuration and structure, producing 32 output channels with 16 input channels. The third convolution layer has the same configuration as the first and second ones, receiving 32 input channels and producing 64 channels. The output is then passed to an adaptive pooling layer to fix the dimension into 4x4. Lastly, the regression head consists of two linear layers and a ReLU activation function. The output features are then flattened into a 1D tensor and passed to the first linear layer with an input of 1024 and an output of 64, followed by a ReLU, then passed to the second linear layer with an input of 64 and an output of 1 so it will only produce one output to estimate the SNR value.

All the convolution layers use a kernel size of 3 because it is commonly used in other deep learning models and can capture local feature patterns while keeping computational resources manageable. The max pooling size is 2. Each time the output from the convolution layer is passed to max pooling, the size of the feature map is reduced by two. This forms hierarchical learning, as each feature map differs at each layer. The adaptive pooling layer can accept any feature map size output from the convolutional layer. It only ensures the feature map is 4 x 4 before passing it to the regression head. Figure 2 shows the architecture of the CalibNet.

3.2 Calibration-Map Learning: Bridging Classical ACF and CNNs

The calibration map is a linear regression-based mathematical model developed to accurately relate classical SNR values to the corresponding ACF SNR values. Linear regression is based on both values to get the perfect fit line optimal when training the model. The calibration map ensures that the predicted ACF SNR value closely aligns with the classical SNR value. Moreover, it can also ensure the predicted value's accuracy and reliability. Both classical SNR and ACF SNR values used for calibration were computed from the train set.

Classical SNR is a conventional definition of SNR based on pixel intensity information. It is commonly used in image processing and communication fields. Equations (1) and (2) show the equation of the classical SNR.

$$SNR_{classical}(dB) = 10 \, log_{10} \left(\frac{\mu^2}{\sigma^2} \right) \tag{1}$$

$$SNR_{classical}(dB) = 20 \, log_{10} \left(\frac{\mu}{\sigma} \right) \tag{2}$$

where μ is the mean pixel intensity, and σ is the standard deviation of the noise image. (1) is commonly used for power ratio, while (2) applies to amplitude ratio. Thus, (2) is used in this paper.

Start

SEM Dataset

Split the dataset into train, validation and test set with 60:20:20 ratio

Corrupt the SEM Image with Gaussain noise variance ranging from 0.001 to 0.01

Train set

Calculate the actual SNR (classical)

Calculate the autocorrelation function SNR (center slice 1D ACF)

Fit linear regression calibration (ACF ≈ a * classical SNR + b) using TRAIN SET ONLY

Use this fixed linear calibration (a, b) to adjust labels on train, validation, and test sets

Train CalibNet using calibrated train set

Evaluate the validation loss during training using validation set

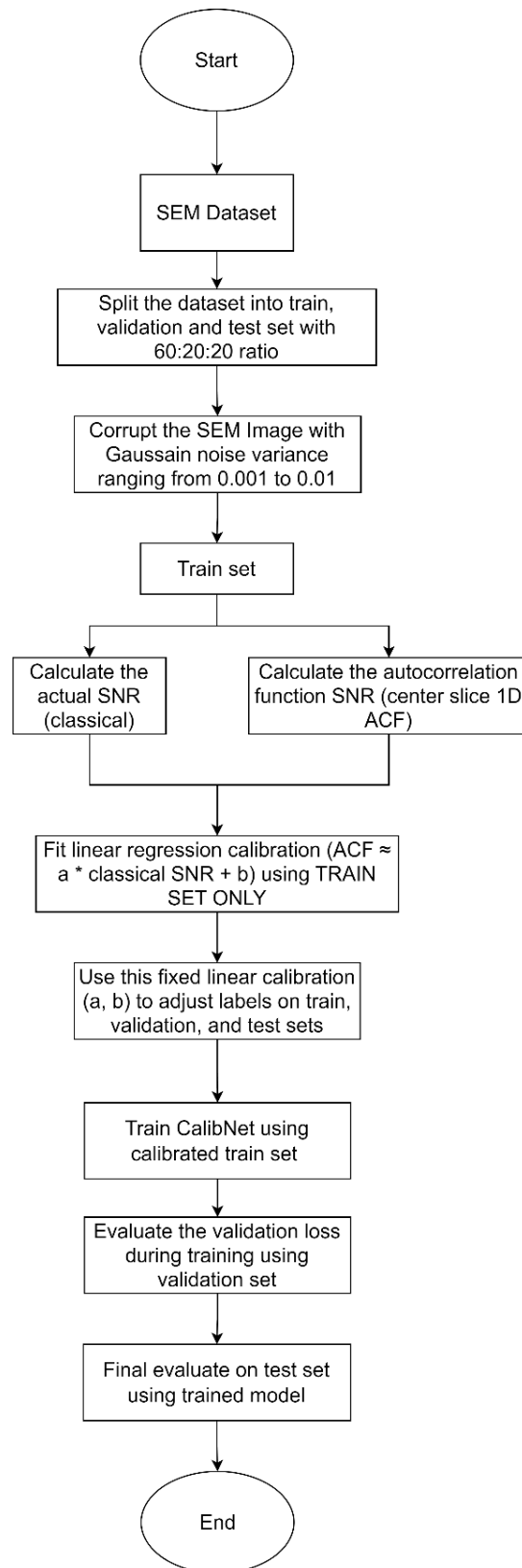Final evaluate on test set using trained model
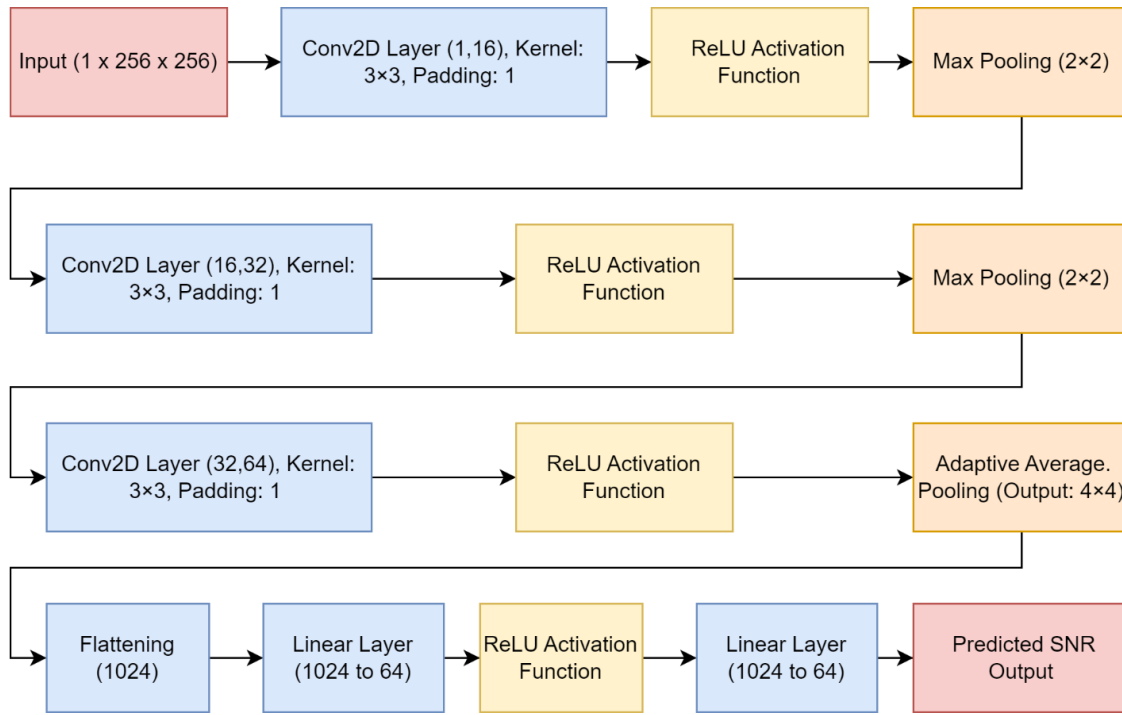
End

Figure 1. The Flowchart of the Process

Figure 2. The Architecture of the CalibNet

ACF SNR is based on the autocorrelation function to estimate the SNR value. The SEM image undergoes a Fast Fourier Transform (FFT) and subsequently shifts to obtain a two-dimensional (2D) ACF. This 2D ACF is then center-sliced to generate a one-dimensional (1D) ACF graph, which shows the peak value at lag 0. The total image signal consists of the original signal and Gaussian noise shown in Equation (3).

$$Total\ Signal = signal + Gaussian\ noise \tag{3}$$

Gaussian noise is additive noise and thus relevant for this analysis. The ACF SNR ratio requires only one pair of images, the original and corresponding noise-image, to estimate the SNR ratio. The difference between their peak values at lag zero is computed using Equation (4).

$$SNR_{ratio} = \frac{h^{NF}(0,y) - \mu^2}{h(0,y) - h^{NF}(0,y)} \tag{4}$$

where h^{NF} is the peak value from the autocorrelation of the noise-free image (original), μ is the mean intensity of the pixel of the original image and $h(0,y)$ is the peak value from the autocorrelation of the noise-corrupted image. After computed the SNR_{ratio} from (4), the value is converted to decibels (dB) using Equation (5).

$$SNR_{ACF}(dB) = 20\log_{10}(SNR_{ratio}) \tag{5}$$

After calculating both the classical and ACF SNR values, linear regression is performed to determine the calibration parameters a and b. These parameters are used in Equation (6), which shows the calibration equation.

$$SNR_{classical} \approx a \cdot SNR_{ACF} + b \tag{6}$$

The accuracy of these calibration parameters is crucial, as incorrect values could compromise the reliability of the entire calibration model. Algorithm 1 shows the CalibNet in estimating SNR value in SEM images.

Algorithm 1: CNN-Based Calibration for SNR Estimation in SEM Images

---

Step Procedure

1   **Initialization & Configuration**

   • Import required libraries (e.g., PyTorch, NumPy, Pandas).

   • Set up training configurations (batch size, epochs, learning rate, device).

2   **Define Utility Functions**

   • Functions for saving model weights.

3   **Dataset Loading & Splitting**

   • Load SEM images and corresponding SNR labels (ACF-based and classical) from Excel files.

   • Split the dataset into training (60%), validation (20%), and test (20%) subsets.

4   **Linear Regression Calibration**

   • Perform linear regression to establish a mapping from ACF-based SNR to classical SNR:

   SNR_classical = a × SNR_acf + b

   • Evaluate regression performance using coefficient of determination (R^2).

5   **Dataset Construction**

   • Create a custom dataset class to load SEM images and apply preprocessing (resize to 256×256, grayscale conversion).

   • Generate calibrated labels using the linear regression parameters (a and b).

6   **Model Definition**

   • Define CNN architecture with convolutional layers, ReLU activations, pooling layers, and fully connected layers for regression.

7   **Training Setup**

   • Prepare data loaders for training and validation sets.

   • Select an optimiser (e.g., AdamW) and define Mean Squared Error (MSE) as the loss function.

8   **Training and Validation**

   • For each epoch:

   - Train the model using the training set to update weights via backpropagation.

   - Validate model performance on the validation set.

   - Save the model checkpoint when validation loss improves.

9   **Testing**

   • Load the best-performing model based on validation loss.

   • Predict SNR values on the test dataset.

   • Compute evaluation metrics: MAE, Mean Squared Error (MSE), RMSE, MAPE, and R^2 score.

10   **Visualisation of Results**

   • Plot predictions vs. actual values, residual plots, histograms, and boxplots to analyse model performance.

No published SEM study has blended the classical pixel-intensity SNR (Equation (2)) with the ACF-based SNR (Equation (5)) into a single target value before deep learning. This paper's training set fits with a linear calibration map (Equation (6)). The resulting scalar serves as the ground-truth label for CalibNet, so the network predicts a single image's SNR.

4. EXPERIMENTAL RESULTS, ANALYSIS, AND DISCUSSIONS

4.1 Dataset

Two SEM datasets, namely the Biofilm SEM dataset [30] and the NFFA-EUROPE SEM dataset [31], were used to train, validate and test the CalibNet.

The Biofilm SEM dataset is the first dataset captured from biofilms on indium tin oxide electrodes, stored in Tagged Image File (TIF) format. It consists of 67 images. The NFFA-EUROPE SEM dataset is the second dataset used in this paper. It consists of 961 biological SEM images stored in Joint Photographic Experts Group (JPG) format. The selection of these datasets ensures sufficient diversity in image characteristics, noise distribution, and sample type, enabling robust evaluation of CalibNet performance.

Both datasets did not specify the SEM equipment models used for image acquisition. However, given the clarity and quality of the images provided, it can be assumed that they were captured under standard SEM operating conditions, which are suitable for typical research applications involving minimal imaging artefacts and moderate noise levels. Each image from both datasets was resized to 256 x 256 pixels to standardise the training, validation and testing processes and ensure they are grayscale. After that, each image was corrupted with Gaussian noise variance ranging from 0.001 to 0.01. Table 3 shows the number of images in each dataset before and after being corrupted with Gaussian noise.

Table 3. Number of Images in Each Dataset Before and After Being Corrupted with Gaussian Noise

Dataset	Number of Images in Original Dataset	Number of Images in Dataset After Corrupted with Gaussian noise variance
Biofilm SEM dataset [30]	67	670
NFFA-EUROPE SEM dataset [31]	961	9610

The noise levels were selected to simulate realistic conditions in SEM imaging. Noise levels higher than 0.01 were not included because SEM images would become excessively corrupted and lose critical details. This makes the SEM images less realistic and impractical for SNR estimation. Each dataset was then split into three subsets, such as training, validation, and test set, with a ratio of 60:20:20 respectively. The seed used for randomisation in splitting the dataset is 42, so the splitting can be reproduced. Table 4 shows the number of images from each dataset in the training, validation, and test sets.

Table 4. Number of Images from Each Dataset in the Train, Validation, and Test Sets

Dataset	Train Set	Validation Set	Test Set
Biofilm SEM dataset	404	134	134
NFFA-EUROPE SEM dataset	5766	1922	1922

4.2 Model Setting

The deep learning model and classical methods used for comparison were coded in Python. The deep learning model was developed using Pytorch. The training ran for 100 epochs at a learning rate of 0.001. The batch size is 32, and the grayscale image size is 256 x 256 pixels. The loss function used in this paper was the mean squared error (MSE) loss function, as it is commonly used in regression tasks. The optimiser chosen was Adaptive Moment Estimation with

decoupled weight decay (AdamW) with the weight decay set to 0.00001. The training was performed on an RTX2080 Ti GPU with 11 GB of memory.

4.3 Method Used for Comparison

Five methods were used to compare with the CalibNet performances. These methods were chosen to show the effectiveness and robustness of CalibNet in estimating the SNR value.

The Classical method is the conventional method that computes the SNR value shown in (2). The ACF method is an autocorrelation-based method that computes the SNR value, as shown in (4). The Nearest Neighbor (NN) ACF method is autocorrelation-based but takes the nearest point adjacent to lag zero. It uses (4) by replacing the $h(0, y)$ to compute the SNR ratio and the SNR value is calculated using (5).

The first-order linear interpolation (FOLI) ACF method is also autocorrelation-based but differs from the NN ACF method. It estimates the peak value by combining the first two nearest points adjacent to the peak and replacing the $h(0, y)$ in (4) to compute the SNR ratio. After that, the SNR value is calculated using (5). The Quarsig ACF method is one of the recent autocorrelation-based methods. It uses a combination of quadratic and sigmoid functions to estimate the SNR ratio. The SNR value is computed using (5).

4.4 Results and Discussions

The performance of the proposed CalibNet was evaluated by comparing the five other methods (ACF, QSE, NN-ACF, LI-ACF, and baseline Classical SNR). Table 5 compares Classical SNR, CalibNet, and four conventional methods on selected test images in the Biofilm SEM dataset. The CalibNet predicted that the SNR value is nearest to the classical SNR, clearly outperforming all the methods. The QSR showed the worst estimation SNR because all the SNR values are negatives.

Table 5. Comparison of Classical SNR, CalibNet, and Four Conventional Methods on Selected Test Images in Biofilm SEM Dataset

No.	Actual ACF SNR (dB)	Classical SNR (dB)	CalibNet (dB)(Proposed)	QSE (dB)	NN (dB)	LI (dB)
1	15.90	6.72	10.90	-26.91	8.21	23.55
2	-0.67	11.63	12.80	-32.95	-5.81	-0.57
3	-12.85	12.89	14.68	-31.36	-19.42	-17.33
4	-5.15	12.54	13.47	-24.92	-8.91	-6.81
5	4.80	16.87	11.96	-7.41	2.47	5.94
6	-9.84	12.05	13.86	-25.78	-12.55	-8.81
7	14.84	14.30	10.67	-25.75	0.07	11.03
8	5.21	9.65	11.70	-26.25	-0.76	6.19
9	-5.43	15.39	13.57	-21.37	-7.13	-3.97
10	5.68	14.30	12.08	-42.30	-3.82	3.02

Table 6 compares classical SNR, CalibNet, and four conventional methods on selected test images in the NFFA-EUROPE SEM dataset. CalibNet shows its strength in estimating the SNR value closest to the classical SNR value, and it outperforms all the methods. The QSE again shows weakness in estimating SNR by getting a negative SNR value. This shows that QSE struggles under noise conditions.

Table 6. Comparison of Classical SNR, CalibNet, and Four Conventional Methods on Selected Test Images in NFFA-EUROPE SEM Dataset

No.	Actual ACF SNR (dB)	Classical SNR (dB)	CalibNet (Proposed)	QSE (dB)	NN (dB)	LI (dB)
1	-9.33	14.68	9.63	-27.67	-14.03	-8.58
2	-38.39	5.93	8.86	-23.64	-23.38	-22.87
3	-4.21	13.71	9.40	-29.34	-7.41	-4.02
4	-18.31	9.41	9.12	-22.85	-16.28	-15.26
5	-42.04	8.99	9.14	-31.27	-33.04	-32.41
6	-20.39	10.75	9.24	-42.52	-23.95	-20.48
7	14.74	11.85	9.86	-9.81	8.81	16.51
8	-44.98	7.58	8.99	-28.59	-31.11	-30.16
9	27.48	4.50	10.42	-0.73	18.25	29.36
10	-6.95	6.07	9.48	-21.38	-9.20	-5.45

Table 7 shows the quantitative metrics of all the methods in the Biofilm SEM dataset. CalibNet has the lowest MAE, RMSE, MAPE and the highest R^2 value among all the methods,   showing that CalibNet has the most accurate and consistent SNR estimation. The QSE has the highest MAE, RMSE, MAPE and extremely low negative R^2 value. The results show that QSE performed the worst in estimating SNR value.

Table 7. Quantitative Metrics of All the Methods in Biofilm SEM Dataset

Method	MAE	RMSE	MAPE (%)	R^2
CalibNet	2.97	3.63	40.84	-0.03
QSE	32.53	34.39	358.80	-92.74
NN	23.90	26.80	278.68	-56.29
LI	22.97	25.71	285.86	-51.22
Actual ACF SNR	24.60	28.19	302.56	-60.98

Table 8 shows the quantitative metrics of all the methods in the NFFA-EUROPE SEM dataset. CalibNet has the lowest MAE, RMSE, MAPE and the highest R^2 value among all the methods, showing that CalibNet has the most accurate and consistent SNR estimation. The QSE has the highest MAE, RMSE, MAPE and extremely low negative R^2 value. The results show that QSE performed the worst in estimating SNR value.

Table 8. Quantitative Metrics of All the Methods in the NFFA-EUROPE SEM Dataset

Method	MAE	RMSE	MAPE (%)	R^2
CalibNet	2.46	3.13	30.23	0.19
QSE	36.40	38.16	321.76	-122.05
NN	17.78	20.77	143.21	-34.89
LI	15.34	18.41	131.86	-28.33
Actual ACF SNR	14.54	17.37	125.51	-24.01

When comparing the performance of the CalibNet in two datasets, the second dataset showed improvement, with lower MAE (2.46 vs 2.97), RMSE (3.13 vs 3.63), and MAPE (30.23% vs. 40.84%), and a better R^2 value (0.19 vs. -0.03). The QSE method performed worse on the second dataset, with much higher metrics errors and a significantly poorer R^2 (-122.05 vs. -92.74). This indicates that CalibNet is more stable and reliable when applied to different SEM datasets.

Table 9 shows the results of paired t-tests comparing CalibNet to other conventional methods in the Biofilm SEM dataset. CalibNet achieved the lowest errors compared to all other methods with $p<0.01$. The QSE has the highest difference in performance compared to CalibNet. It has a mean difference of 29.42 dB lower error, followed by Actual ACF SNR (21.63 dB), NN (20.91 dB), and LI (19.99 dB). These results show that CalibNet estimates the SNR values more accurately.

Table 9. The Results of Paired T-Tests Comparing CalibNet to Other Conventional Methods in Biofilm SEM Dataset

Method	CalibNet MAE	Method MAE	Mean Difference	t-statistic	p-value	Significance	N
QSE	3.11	32.53	-29.42	-28.45	6.35924E-55	(p<0.01)	120
NN	2.99	23.90	-20.91	-19.59	1.27967E-40	(p<0.01)	131
LI	2.99	22.97	-19.99	-19.70	5.44274E-41	(p<0.01)	132
Actual ACF SNR	2.97	24.60	-21.63	-17.68	9.77543E-37	(p<0.01)	134

Table 10 shows the results of paired t-tests comparing CalibNet to other conventional methods in the NFFA-EUROPE SEM dataset.

CalibNet achieved the lowest errors compared to all other methods with $p<0.01$, the same as the Biofilm dataset. The QSE has the highest difference in performance compared to CalibNet, which is the same as the first dataset. It has a mean difference of 33.94 dB lower error, the worst among other methods. These results show that CalibNet estimates the SNR values more accurately.

Table 10. The Results of Paired T-Tests Comparing CalibNet to Other Conventional Methods In the NFFA-EUROPE SEM Dataset

Method	CalibNet MAE	Method MAE	Mean Difference	t-statistic	p-value	Significance	N
QSE	2.46	36.40	-33.94	-121.70	0	(p<0.01)	1725
NN	2.47	17.78	-15.31	-61.25	0	(p<0.01)	1904
LI	2.46	15.34	-12.88	-53.86	0	(p<0.01)	1863
Actual ACF SNR	2.46	14.54	-12.08	-53.36	0	(p<0.01)	1922

Based on the overall results, CalibNet demonstrated strong performances and outperformed all the other methods. These results suggest that the deep learning method can perform better than the classical methods by extracting the image features. The classical techniques and statistical analysis result confirms this performance in estimating SNR value. Deep learning addressed the gap between classical and deep learning by automatically calculating the SNR value. However, this study is limited to a moderate noise variance range (0.001 to 0.01), chosen to simulate realistic SEM conditions without compromising image integrity.

5. CONCLUSION

In this paper, a deep learning model, CalibNet, was successfully developed for accurately estimating the SNR value in SEM images. CalibNet outperformed all the classical autocorrelation-based methods. It had the lowest MAE, RMSE, MAPE and highest R^2. Moreover, the results also showed that the SNR value estimated by CalibNet is the closest to the classical SNR. Statistical analysis confirmed the performance improvement ($p<0.001$) compared to all classical methods. CalibNet can bring benefits with its high accuracy to real-world applications, including image quality assessment and quantitative analyses in biological and materials science fields.

The paper still has room for improvement. Future work could explore other models, such as transformer-based architectures, attention mechanisms, or hybrid CNN-RNN models, to better address SNR estimation tasks. Additionally, the calibration map can be enhanced by applying advanced calibration techniques such as polynomial regression, non-linear regression, or machine-learning-based calibration to achieve more accurate SNR estimations. Furthermore, CalibNet could be extended for real-time applications, allowing immediate and practical estimation of SNR values for SEM images.

AUTHOR CONTRIBUTIONS

Kai Liang Lew: Conceptualization, Data Curation, Methodology, Validation, Writing – Original Draft Preparation;
Kok Swee Sim: Project Administration, Supervision, Writing – Review & Editing;
Shing Chiang Tan: Writing – Review & Editing.

The datasets used in this study, including the original datasets and their modifications for SNR estimation tasks, have been uploaded to Zenodo.

CONFLICT OF INTERESTS

No conflicts of interest were disclosed.

ETHICS STATEMENTS

Our publication ethics follow The Committee of Publication Ethics (COPE) guidelines. https://publicationethics.org/.

REFERENCES

[1]   N. S. Kamel and K. S. Sim, "Image signal-to-noise ratio and noise variance estimation using autoregressive model," *Scanning*, vol. 26, no. 6, pp. 277–281, Nov. 2004, doi: 10.1002/sca.4950260605.

[2]   K.-C. Chang *et al.*, "Integrating ultraviolet sensing and memory functions in gallium nitride-based optoelectronic devices," *Nanoscale Horiz.*, vol. 9, no. 7, pp. 1166–1174, 2024, doi: 10.1039/D3NH00560G.

[3]   G. Schinazi, E. J. Price, and D. A. Schiraldi, "Chapter 3 - Fire testing methods of bio-based flame-retardant polymeric materials," in *Bio-Based Flame-retardant Technology for Polymeric Materials*, Y. Hu, H. Nabipour, and X. Wang, Eds., Elsevier, pp. 61-95, 2022, doi: 10.1016/B978-0-323-90771-2.00009-2.

[4]   H. S. Samuel and F. Makong Ekpan, "The use of scanning electron microscopy SEM for medical application: A mini review," *Eurasian Journal of Science and Technology.*, no. Online First, May 2024, doi: 10.48309/ejst.2024.449519.1134.

[5]   E. Oho, N. Ichise, W. H. Martin, and K.-R. Peters, "Practical method for noise removal in scanning electron microscopy," *Scanning*, vol. 18, no. 1, pp. 50–54, Jan. 1996, doi: 10.1002/sca.1996.4950180108.

[6]   M. Prasad and D. Joy, "Is SEM noise Gaussian?," *Microscopy and Microanalysis*, vol. 9, pp. 982–983, Aug. 2003, doi: 10.1017/S1431927603444917.

[7]   J. Chen, X. Jang, K. Goto, T. Takashi, and Y. Toyoda, "A flexible deep learning based approach for SEM image denoising," in *Metrology, Inspection, and Process Control XXXVIII*, M. J. Sendelbach and N. G. Schuch, Eds., San Jose, United States: SPIE, pp. 127, Apr. 2024, doi: 10.1117/12.3011135.

[8]   D. Roldan, C. Redenbach, K. Schladitz, C. Kubel, and S. Schlabach, "Image quality evaluation for FIB-SEM images," *Journal of Microscopy*, vol. 293, no. 2, pp. 98-117, Feb. 2024, doi: 10.1111/jmi.13254.

[9]   S. H. Shirazi, N. U. Haq, K. Hayat, S. Naz, and I. U. Haque, "Curvelet based offline analysis of SEM images," *PLoS ONE*, vol. 9, no. 8, pp. e103942, Aug. 2014, doi: 10.1371/journal.pone.0103942.

[10]   I. B. Montenegro, K. Prikoszovich, S. Lee, K. Quiring, J. Zimmerman, and C. Kirchlechner, "Redundant cross-correlation for drift correction in SEM nanoparticle imaging," *arXiv*: arXiv:2410.23390, Oct. 30, 2024, doi: 10.48550/arXiv.2410.23390.

[11]   N. Marturi, S. Dembele, and N. Piat, "Scanning electron microscope image signal-to-noise ratio monitoring for micro-nanomanipulation," *Scanning*, vol. 36, no. 4, pp. 419-429, Jul. 2014, doi: 10.1002/sca.21137.

[12]   A. Rodriguez-Sanchez, A. Thompson, L. Korner, N. Brierley, and R. Leach, "Review of the influence of noise in X-ray computed tomography measurement uncertainty," *Precision Engineering*, vol. 66, pp. 382-391, Nov. 2020, doi: 10.1016/j.precisioneng.2020.08.004.

[13]   K. S. SIM, M. A. KIANI, M. E. NIA, and C. P. TSO, "Signal-to-noise ratio estimation on SEM images using cubic spline interpolation with Savitzky-Golay smoothing," *Journal of Microscopy*, vol. 253, no. 1, pp. 1–11, Jan. 2014, doi: 10.1111/jmi.12089.

[14]   A. E. Ilesanmi and T. O. Ilesanmi, "Methods for image denoising using convolutional neural network: a review," *Complex & Intelligent Systems*, vol. 7, no. 5, pp. 2179–2198, Oct. 2021, doi: 10.1007/s40747-021-00428-4.

[15]   J. Heine, E. Fowler, and M. B. Schabath, "Fourier analysis of signal dependent noise images," *Scientific Reports*, vol. 14, no. 1, pp. 30686, Dec. 2024, doi: 10.1038/s41598-024-78299-1.

[16]   M. Taassori, "Enhanced wavelet-based medical image denoising with Bayesian-optimized bilateral filtering," *Sensors*, vol. 24, no. 21, pp. 6849, Oct. 2024, doi: 10.3390/s24216849.

[17]   A. E. Ilesanmi and T. O. Ilesanmi, "Methods for image denoising using convolutional neural network: a review," *Complex & Intelligent Systems*, vol. 7, no. 5, pp. 2179–2198, Oct. 2021, doi: 10.1007/s40747-021-00428-4.

[18]   S. S. M. M. Rahman, M. Salomon, and S. Dembele, "Towards scanning electron microscopy image denoising: a state-of-the-art overview, benchmark, taxonomies, and future direction," *Machine Vision and Applications*, vol. 35, no. 4, pp. 87, Jul. 2024, doi: 10.1007/s00138-024-01573-9.

[19]   P. Jain and V. Tyagi, "LAPB: Locally adaptive patch-based wavelet domain edge-preserving image denoising," *Information Sciences*, vol. 294, pp. 164–181, Feb. 2015, doi: 10.1016/j.ins.2014.09.060.

[20] L. Chang, X. Feng, X. Li, and R. Zhang, "A fusion estimation method based on fractional Fourier transform," *Digital Signal Processing*, vol. 59, pp. 66–75, Dec. 2016, doi: 10.1016/j.dsp.2016.07.016.

[21] A. De Stefano, P. R. White, and W. B. Collis, "Training methods for image noise level estimation on wavelet components," *EURASIP Journal on Advances in Signal Processing*, vol. 2004, no. 16, pp. 405209, Dec. 2004, doi: 10.1155/S1110865704401218.

[22] K. S. Sim, Z. X. Yeap, F. Ting, and C. Tso, "The performance of adaptive tuning piecewise cubic hermite interpolation model for signal-to-noise ratio estimation," *International Journal of Innovative Computing, Information and Control*, vol. 14, pp. 1787–1804, Oct. 2018, doi: 10.24507/ijicic.14.05.1787.

[23] X. Liu, M. Tanaka, and M. Okutomi, "Single-image noise level estimation for blind denoising," *IEEE Transactions on Image Processing*, vol. 22, no. 12, pp. 5226–5237, Dec. 2013, doi: 10.1109/TIP.2013.2283400.

[24] K. L. Lew, K. S. Sim, and S. C. Tan, "Single image estimation techniques for SEM imaging system," *JOIV International Journal on Informatics Visualization*, vol. 9, no. 1, pp. 104, Jan. 2025, doi: 10.62527/joiv.9.1.3505.

[25] W. Ahmed, S. Khan, A. Noor, and G. Mujtaba, "Deep learning-based noise type classification and removal for drone image restoration," *Arabian Journal for Science and Engineering*, vol. 49, no. 3, pp. 4287–4306, Mar. 2024, doi: 10.1007/s13369-023-08376-6.

[26] K. S. Sim, C. C. Lim, S. C. Tan, and C. K. Toa, "Deep convolutional neural network for SEM image noise variance classification," *Engineering Letters*, vol. 31, no. 1, 2023.

[27] F. Liu, Q. Song, and G. Jin, "The classification and denoising of image noise based on deep neural networks," *Applied Intelligence*, vol. 50, no. 7, pp. 2194–2207, Jul. 2020, doi: 10.1007/s10489-019-01623-0.

[28] P. Pawar, B. Ainapure, M. Rashid, N. Ahmad, A. Alotaibi, and S. S. Alshamrani, "Deep learning approach for the detection of noise type in ancient images," *Sustainability*, vol. 14, no. 18, pp. 11786, Sep. 2022, doi: 10.3390/su141811786.

[29] W. Ahmed, Z. H. Khand, S. Khan, G. Mujtaba, M. A. Khan, and A. Waqas, "Multi-type image noise classification by using deep learning," *International Journal of Computer Science and Network Security*, vol. 24, no. 7, pp. 143–147, Jul. 2024, doi: 10.22937/IJCSNS.2024.24.7.17.

[30] B. N. Orcutt, "Scanning Electron Microscopy (SEM) photographs of biofilms on indium tin oxide electrodes from cathodic poised potential experiments with subsurface crustal samples from CORK borehole observatories at North Pond on the Mid-Atlantic Ridge during R/V A." *Biological and Chemical Oceanography Data Management Office (BCO-DMO).*, Feb. 03, 2020, doi: 10.1575/1912/bco-dmo.780261.1.

[31] R. Aversa, M. H. Modarres, S. Cozzini, and R. Ciancio, "NFFA-EUROPE - 100% SEM dataset." *NFFA-EUROPE Project*, 2018, doi: 10.23728/b2share.80df8606fcdb4b2bae1656f0dc6db8ba.

BIOGRAPHIES OF AUTHORS

Kai Liang Lew received the B. Eng. (Hons) degree and M.Sc. in Engineering from Multimedia University, Malacca, Malaysia in 2019 and 2022, respectively. He is currently pursuing a Ph.D. degree in engineering at Multimedia University. His research interests include rehabilitation, deep learning, and signal processing. He can be contacted at email: sksbg2022@gmail.com.

Kok Swee Sim is a Professor at Multimedia University, Malaysia, collaborates extensively with local and international institutions and hospitals. He holds over 18 patents and 70 copyrights, and is a fellow of the Institution of Engineers, Malaysia (IEM) and the Institution of Engineering and Technology (IET). His numerous accolades include the Japan Society for the Promotion of Science (JSPS) Fellowship (2018), Top Research Scientists Malaysia (TRSM) (2014), multiple Korean Innovation and Special Awards, and several TM Kristal and WSIS Prizes. He can be contacted at email: kssim@mmu.edu.my.

Shing Chiang Tan earned his B.Tech. (Hons.) and M.Sc. (Eng.) from Universiti Sains Malaysia in 1999 and 2002, and his Ph.D. from Multimedia University (MMU), Malaysia, in 2008. He's currently a professor at MMU's Faculty of Information Science and Technology, Malaysia. His research focuses on computational intelligence, deep learning, data classification, condition monitoring, fault detection, stroke rehabilitation, and biomedical applications. He was awarded the Matsumae International Foundation Fellowship, Japan, in 2010. He can be contacted at email: sctan@mmu.edu.my.